



IJRASET

International Journal For Research in
Applied Science and Engineering Technology



INTERNATIONAL JOURNAL FOR RESEARCH

IN APPLIED SCIENCE & ENGINEERING TECHNOLOGY

Volume: 10 Issue: V Month of publication: May 2022

DOI: <https://doi.org/10.22214/ijraset.2022.43510>

www.ijraset.com

Call:  08813907089

E-mail ID: ijraset@gmail.com

A Power Quality Improved EV Charger by Using Bridgeless CUK Converter

Ganesh Prasad Reddy Jonnala¹, Sairam Mudigonda², Mohan Dharma Nayak Malavathu³, Nagesh Mala⁴, Supriya Velupula⁵

¹Professor and Dean of academics, Sree Vahini Institute of Science and Technology, Tiruvuru, A.P

^{2, 3, 4, 5}UG Students of Sree Vahini Institute of Science and Technology, Tiruvuru A.P

Abstract: This study designs and develops an improved bridgeless (BL) Cuk converter-based electric vehicle (EV) battery charger with a high-power factor and higher efficiency. It offers a low-cost, high-power-density-based charging solution for EVs. This charger has fewer components functioning during a single switching cycle, which decreases the extra conduction loss experienced by the typical charger's diode bridge rectifier. As a result, it boosts the charger's efficiency. The suggested topology also avoids the undesired capacitive coupling loop and unwanted conduction via the body diode of the inactive switch in the previously developed BL Cuk converter. This considerably enhances the charger's efficiency. A flyback converter synchronises the orders for constant current and constant voltage charging. The suggested charger draws a sinusoidal current from an alternating current main, and the overall harmonic distortion in the supply current is kept within the IEC 61000-3-2 requirements. The suggested charger's increased efficiency and power quality indices are studied to verify its good charging performance under all operational situations.

Keywords: Bridgeless (BL) Cuk converter, discontinuous conduction mode (DCM), flyback converter, power factor correction (PFC), and power quality are all terms used to describe a battery charger (PQ).

I. INTRODUCTION

Battery-powered electric vehicles (BEVs) already outnumber traditional gasoline-powered cars in terms of the long-term growth of the modern transportation industry [1]. An ac-dc converter-based on-board or off-board charger is a critical piece of electric vehicle supporting equipment for facilitating battery charging in BEVs (EV). Various off-board and on-board topologies of EV battery chargers with unidirectional or bidirectional configurations are studied in the literature under level 1, level 2, or level 3 categories. An off-board power supply, in addition to high power density and a compact form factor.

To increase energy consumption when charging, chargers must have improved power quality (PQ) features. A standard EV charger with a diode bridge rectifier (DBR) draws a peaky current from the mains, lowering the input power factor (PF) and causing up to 55.3 percent total harmonic distortion (THD). Table I shows the battery rating and specs of the EV under test. The recorded waveforms clearly show that the performance of the DBR fed charger does not meet international criteria such as the IEC 6100-3-2 standard. To address these issues, better PQ-based EV chargers are being intensively researched in the literature. These chargers draw a sinusoidal input current with a high PF, and the output voltage is stiffly controlled at a constant amount. Several topologies of front-end power-factor-correction (PFC) converters are studied in the literature for EV chargers, depending on whether they are off-board or on-board. This relates to several on-board EV chargers with substantial advantages in terms of power density and efficiency. However, because of the lower vehicle weight and capacity to charge at high power levels, an off-board design is a more viable choice. Different PFC converter topologies with interleaved input at the front end and zero-voltage-switching approaches are presented. Interleaving two-phase inputs has the advantage of lowering output ripple current and reducing the size of the inductor. Furthermore, the semiconductor devices are run in parallel, resulting in lower conduction losses. However, unlike the traditional boost PFC converter, interleaved PFC converters do not provide a remedy for poor thermal use of PFC switches. This paper discusses an LLC resonant converter fed EV charger, which has the added benefit of reduced electromagnetic interference (EMI) noise and switching loss. However, the resonant converter's complicated mathematical analysis renders it unsuitable for EV charging across a large input voltage range. A full-bridge PFC converter appears to be the most promising option for EV chargers, but building separate gate drivers for four semiconductor switches increases the size and complexity. As a result, several unidirectional PFC off-board EV chargers are addressed in order to give ease of application while keeping the benefits of high-power density and efficiency.

Using different single-stage and two-stage PFC converters leads to perceptible PQ indices at the input of these chargers. In the literature, many single-stage PFC-converter-based EV charger topologies have been published. Because of its low part count, the single-stage charger is highly dependable. However, the existence of 100-Hz ripple content in the output current necessitates extremely high DC-link capacitance. A two-stage charger with a PFC converter is a widely feasible option in the EV market for medium power levels up to 1 kW. Because of the considerable conduction loss experienced by the four input diodes, the DBR-fed PFC converter reduces the charger's efficiency. As a result, with fewer components conducting during one switching cycle and lower conduction loss, a bridgeless (BL) PFC converter is the most practical approach for improving PQ in an EV charger. Because it can both buck and boost the input voltage, the BL buck–boost converter is the most appealing solution for PFC in EV chargers. We describe and analyse a variety of buck–boost configuration-based converters, including Cuk and SEPIC converters. Despite the fact that the Zeta, Cuk, and SEPIC PFC converters have minimal input current ripple and a large duty cycle fluctuation range, the SEPIC converter, unlike the Cuk converter, has a discontinuous output current. As a result of the minimal ripple in the battery current, the Cuk converter gives more practicable charging characteristics to the battery. Many topologies of the BL-Cuk converter based on the typical PFC Cuk converter are studied in the literature [20–23]. All of these topologies have restrictions in terms of the number of components, losses, efficiency, and coupling requirements, which are explored more below.

- 1) As shown in Fig. 1(b), Topology-1 in [20] has advantages such as lower input current, less EMI, and ease of installation. However, it has a circulating current problem [as shown in Fig. 1(c)], which produces extra losses of two-thirds of the supply voltage owing to the connectivity of two intermediate capacitors, C1 and C2.
- 2) Topology-2 employs a significant number of devices, such as two output capacitors, with the disadvantage of a floating terminal for load between two capacitors at output. Furthermore, because of the placement of switches for the independent half of the supply voltage, as illustrated in Fig. 2, it has the problem of floating neutral (d).
- 3) Topology-3 in [20] is found to be lossy because the body diode of the inactive switch S2 conducts current via Li2 during the positive half cycle of the input voltage, as seen in Fig. 2. (e). As a result, the circuit always incurs some losses across the inactive switch's body diode due to partial return current flow through it during other half-cycle operation.
- 4) The other BL Cuk converters in [21] and [23] are shown in Fig. 2(f) and (g), respectively, and have the same advantages of low component count and lower semiconductor device stress as the typical Cuk converter. However, coupled induction in both the input and output inductors is not conceivable for any of these converters. This may result in greater output and input ripple, which is undesirable for battery service life.

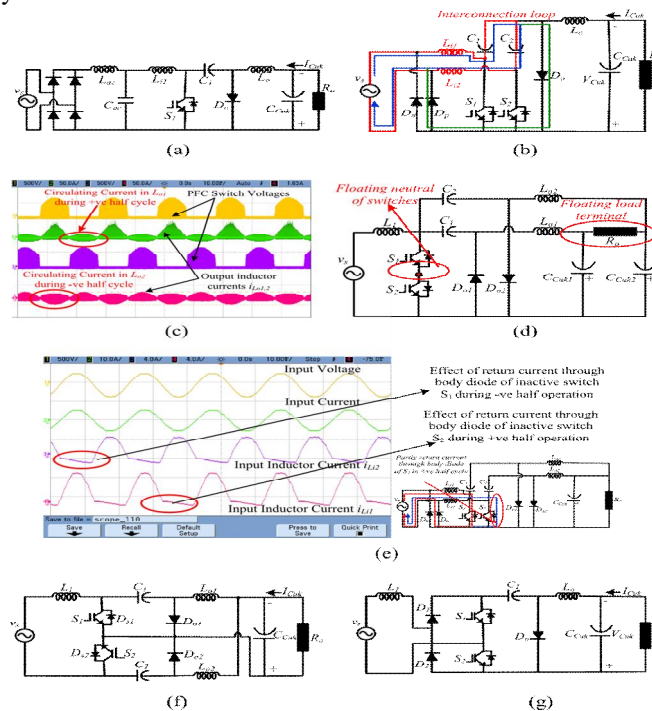


Fig. 2. Different BL Cuk converters. (a) Conventional Cuk converter. (b) Topology-1 [20]. (c) Circulating current due to interconnection of C1 and C2 in topology-1[20]. (d) Topology-2 [20]. (e) Topology-3 with return current [20] through the body diode. (f) Topology in [21]. (g) Topology in [23].

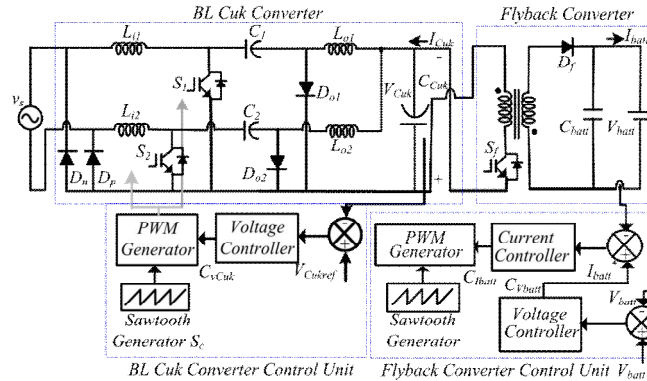


Fig. 3. Proposed BL-Cuk converter-based EV charger configuration

During the constant current (CC) and constant voltage (CV) charging zones, the converter manages the input voltage of the flyback converter, which is used to maintain the required charging current through the battery. A prototype is created, and the increased PQ performance of the proposed EV charger, as defined by the IEC 61000-3-2 standard, is demonstrated during steady state and during broad ac voltage swings.

II. CONFIGURATION AND OPERATION

Figures 3 and 4 depict the configuration and operation of the planned PQ improved EV charger. The Cuk converter cell, consisting of L_{i1} – S_1 – D_{o1} – L_{o1} – D_p , is in operation during the positive half cycle. However, the other Cuk converter cell, L_{i2} – S_2 – D_{o2} – L_{o2} – D_n , is active during the negative half line. For both Cuk converter cells, the input inductors L_{i1} and L_{i2} are set to function in the continuous conduction mode (CCM). However, the output inductors L_{o1} and L_{o2} are designed in such a way that the output diode current, i_d , reaches zero and the converter enters DCM after one switching cycle. The intermediate capacitors C_1 and C_2 are chosen so that the voltage across the capacitors remains constant throughout the switching time. It is worth noting that both switches, S_1 and S_2 , are powered by the same pulse width modulation (PWM) signal, lowering system cost and circuit complexity.

The PFC Cuk converter's output voltage is kept constant by using single-loop voltage feedback control [27], [28], which lowers the charger cost because only one voltage sensor is used. The flyback converter is designed to work in the DCM [29] mode, with a cascaded proportional-integral (PI) controller controlling the battery charging commands during the CC and CV charging periods. The output inductor current in the Cuk converter during PFC in the DCM is depicted in Fig. 4.

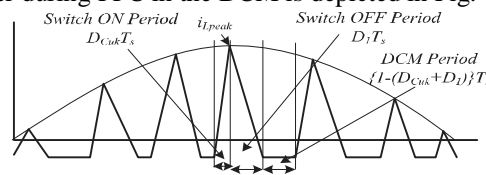


Fig.4. Principle of PFC Operation.

A. Operation of the BL Cuk PFC Converter

Only the positive half cycle of the BL converter is considered due to waveform symmetry, as shown in Fig. 5(a)–(c). The operational phases of the Cuk converter are illustrated in this section to demonstrate how the proposed EV charger works.

1) P-I Mode [0 t DCuk Ts Switch-ON Period]:

When the gate pulse to switch S_1 is applied, the first mode of the positive half-cycle operation (P-I) begins at t_1 . The current flowing through the input inductor L_{i1} increases linearly as the slope of $V_{spk}(t)/L_{i1}$ increases. As the positive line diode D_p is conducting, the current flows via the path v_s – L_{i1} – S_1 – D_p – v_s . Figure 6 depicts the essential switching waveforms associated with all three modes. Through the switch S_1 and the output inductor, L_{o1} , the voltage across the intermediate capacitor C_1 begins to decrease, giving the appropriate load current to the flyback converter. Due to the polarity of the intermediary capacitor voltage, C_1 , the output diode D_{o1} stays in reverse bias during this interval. The peak current stress across switch S_1 during this mode is given as

$$I_{s1pk}(1) = V_{spk} D_{Cuk} T_s \quad (1)$$

where L_{eq} represents the proposed converter's equivalent circuit inductance, i.e., the input inductor L_{i1} and the output inductor L_{o1} . The maximum value of the input alternating voltage is V_{spk} , the ON period for switch S_1 is DC_{Cuk} , and the overall switching time is T_s .

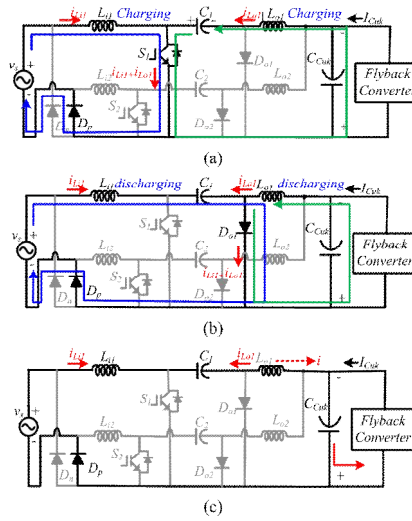


Fig. 5. Circuit operation of the EV charger with BL PFC Cuk converter during the positive half cycle. (a) Mode P-I. (b) Mode P-II. (c) Mode P-III.

2) Mode P-II [Switch OFF Period, $DC_{Cuk} T_s \leq t \leq D_1 T_s$]

When switch S_1 is turned off at instant t_2 , this mode begins. As shown in Fig. 5, the output diode $Do1$ begins to conduct and the voltage across the intermediate capacitor begins to rise as the input inductor $Li1$ begins to release the stored energy via C_1 and $Do1$ (b). The load current is provided by the output inductor $Lo1$, which releases the stored energy via the output diode $Do1$ and dc-link capacitor CC_{Cuk} .

The given equation represents the current i_{Lo1} through the output inductor.

$$\frac{di_{Lo1}}{dt} = \frac{V_{C_{Cuk}}}{L_{o1}} \tag{2}$$

where $V_{C_{Cuk}}$ is the BL Cuk converter's output voltage.

When the current via the output diode becomes zero at instant 3, the switching period finishes. The normalised duty cycle value in this switching mode is determined using the following relation:

$$DC_{Cuk} T_s + D_1 T_s, \text{ which provides } DC_{Cuk} + D_1 = 1. \tag{3}$$

During mode-II operation of the proposed Cuk converter

$$V_{C_{Cuk}} T_{off} = n T_{on} V_s$$

$$T = \frac{n T_{on} V_s}{V_{C_{Cuk}}} \tag{4}$$

When n is the converter's isolation transformation ratio, T_s is the switching time, and T_{on} and T_{off} are the switch-ON and switch-OFF phases. $n = 1$ in the proposed non-isolated Cuk converter. Now, replace $V_s = V_{spk} \sin \omega t$ and dc gain of the converter with $M = V_{C_{Cuk}} / V_{spk}$.

The relationship in (4) is altered as follows:

$$D_1 T_s = \frac{n DC_{Cuk} T_s (V_{spk} \sin \omega t)}{V_{C_{Cuk}}}$$

$$D_1 = \left(\frac{n DC_{Cuk}}{M} \right) \sin \omega t \tag{5}$$

where ω denotes the angular frequency given as $2\pi/T_s$.

3) Mode P-III [DCM Mode, $D_1 T_s \leq t \leq T_s$]:

This is the DCM mode, in which the current through the output diode Do1 becomes zero as the sum of the input and output inductor currents becomes zero. For this, the current through one of the inductors (here, the output inductor) must be reversed, as shown in Fig. 5 (c), or it will become zero before the end of mode-II (instant t_3 in Fig. 6). As seen in Fig. 6, a constant current I passes across the circuit at this time. From their starting levels, the inductor currents undergo a fresh switching cycle: I for i_{Li1} and I for i_{Lo1} . C1 (the intermediate capacitor) continues to charge via the input inductor $Li1$ and output diode Do1. The DCM time period is provided as

$$t_3 - t_4 = T_s - \{(t_2 - t_1) + (t_3 - t_2)\} \tag{6}$$

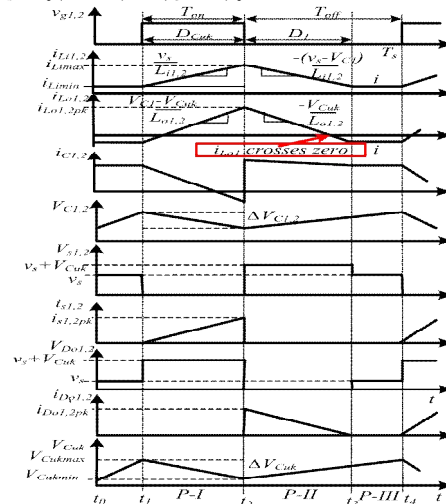


Fig. 6. Associated switching behaviour of the different components over the complete switching cycle.

In the negative half line, the same switching sequence is followed, and at the end of this switching cycle, S2 begins conducting, kicking off the next operating cycle.

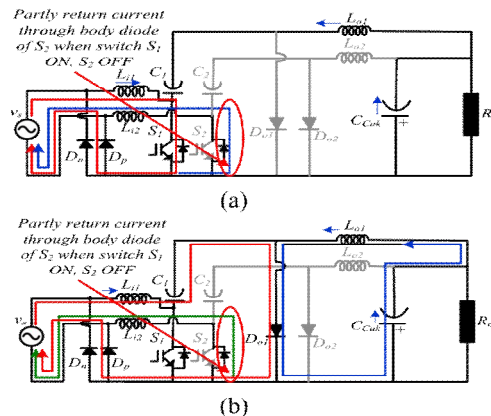


Fig. 7. Operating modes of topology-3 with the conventional control during the positive half line. (a) Switch-ON period. (b) Switch-OFF period.

B. Differential Aspect of the Proposed PFC Converter

The following sections explain the differences between the proposed PFC converter and the BL Cuk topologies 1 and 3 [20].

- 1) The intermediate capacitors in both halves operate independently; because there is no connectivity between C1 and C2, circulation losses are eliminated, resulting in higher charger efficiency.
- 2) Due to the traditional control, the body diode of the inactive switch S2 is always conducting the current during the positive half cycle of the input voltage, as shown in Fig. 2 (e). The following sections explain the differences between the proposed PFC converter and the BL Cuk topologies 1 and 3 [20].

- 3) Due to the traditional control, the body diode of the inactive switch S2 is always conducting the current during the positive half cycle of the input voltage, as shown in Fig. 2 (e). This means that when switch S1 is turned on during the positive half cycle, current flows not only through Dp but also via the body diode of switch S2 and inductor Li2. When switch S1 is turned off, current flows not only through the line diode Dp via the output diode Do1, but also through the inductor Li2 via the body diode, Dp. The same is true for the negative half-cycle operation with switch S2. This occurs when a single PWM signal is applied to only one of the switches during one half, i.e., S1 or S2, and the other switch is maintained completely off for the other half. As a result, as shown in Fig. 7(a) and (b), the circuit always incurs some losses across the body diode of the inactive switch (S1 or S2) due to partially returned current flowing through it during the corresponding half-cycle operation.
- 4) Unlike in Fig. 2, there is no return current through the body diode of inactive switches in the relevant half cycle due to applied control (e). The control of the PFC converter is straightforward due to the use of the same gate drive and control circuitry for each half cycle, i.e., both switches S1 and S2 work in synchronism with the same driver signal. In other words, the same driver signal and interleaved driver signal can be utilised to operate switches S1 and S2 to reduce conduction loss through the body diode of the inactive switches. As a result, losses in the body diode are decreased. The actual operating modes differ slightly from those shown in Figs. 5(a)–(c) with the same driver signal. The preceding fact is supported by Figs. 8(a) and (b), which show the proposed converter operating with the same control signal during the switch-ON and switch-OFF periods during the positive half of the supply cycle, respectively.

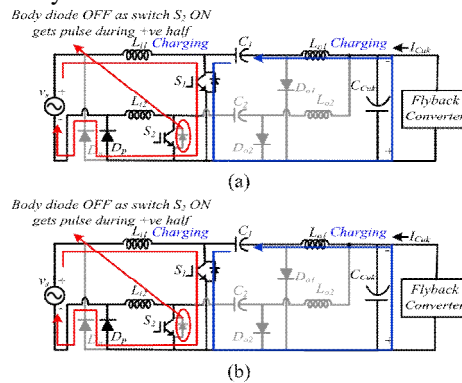


Fig. 8. Operating modes of the proposed converter with same driver signal during the positive half line during (a) switch ON and (b) switch OFF.

C. Operation of the Flyback Converter

The DCM of the high frequency transformer's magnetising inductance is used to examine the operation of the flyback converter (HFT). During mode-I, the current flowing through the magnetic inductance L_{mf} rises linearly and stores energy when the flyback switch S_f is turned on. During this instant, the output diode, D_f , is reverse biased due to the HFT's dot convention. The current flowing through the switch S_f is denoted as

$$i_{Sf} = i_{Lf} = \int_{t_1}^{t_2} V_{C_{uk}} dt + i_{Lf}(0) = \frac{V_{C_{uk}}}{L_f} (t_1 - t_2) + i_{Lf}(0) \quad (7)$$

where $i_{Lf}(0)$ is the current flowing through the magnetising inductance at time t_1 . The maximum current through the switch is calculated as

$$i_{Sf} (D_{fb} T_{sf}) = \frac{V_{C_{uk}} D_{fb}}{L_{ff} f_{sf}} + i_{Lf}(0) \quad (8)$$

where D_{fb} is the needed duty cycle and T_{sf} ($1/f_{sf}$) is the switching period of the flyback converter, which in this article is set at 1/50 kHz. Taking the flyback transformer's transformation ratio as N .

Mode II begins when switch S_f is turned off at instant t_2 . As the polarity of the HFT is reversed during the switch OFF moment and the output diode D_f becomes forward biased, the output power is provided to the battery. The switch current is f and diode voltage V_{Df} are both zero. The current flowing through the magnetising inductance at this time is denoted by

$$i_{Lf} = \frac{1}{L_f} \int_{t_2}^{t_3} (-N V_{batt}) dt + i_{Lf}(D_{fb} T_{sf}) = \frac{(-N V_{batt})}{L_f} (t_3 - t_2) + \frac{V_{C_{uk}} D_{fb}}{L_f f_{sf}} + i_{Lf}(0) \quad (9)$$

where i_{Lf} ($D_{fb} T_{sf}$) denotes the initial current via the magnetising inductance at time t_2 . As a result, the diode current i_{Df} is calculated as

$$i_{Df} = Ni_{Lf} \tag{11}$$

The peak voltage across the switch can be calculated using the equation:

$$V_{Sfm} = VC_{uk} + NV_{batt} = \frac{NV_{batt}}{D_{fb}} \tag{12}$$

This mode terminates at point t_3 . Mode-III, also known as DCM, begins when both the switch and the diode are switched off. At the end of the switching cycle, the stored energy in the magnetising inductance is totally transmitted to the output. In the CC mode, the output capacitor C_{batt} supplies the appropriate battery charging current at this time.

$$i_{Df} = i_{sf} = 0. \tag{13}$$

III. DESIGN OF THE PROPOSED PFC CONVERTER-BASED CHARGER

The cost of the EV charger is directly connected to the PFC converter's sensing needs [30–32]. The CCM's control strategy employs the current multiplier technique to offer intrinsic wave-shaping and dc-link regulation. The CCM requires a greater number of sensors due to the need to sense the output voltage as well as the input voltage and current. The primary benefit of CCM operation is that it reduces current stress on PFC converter switches and components. However, the required sensors are decreased in DCM operation since the control strategy is based on the voltage follower approach and the only quantity to be detected is the converter's output voltage. As a result, the DCM-based design approach is appropriate in the proposed work to reduce cost and complexity. The inherent PFC for the proposed BL Cuk converter in DCM mode is shown below.

The average input and output inductor currents over the switching period T_s are expressed as

$$i_{Li1} = \frac{V_s D_{Cuk} T_s (D_{Cuk} + D_1)}{2L_{i1}} - i \tag{14}$$

$$i_{Lo1} = \frac{V_s D_{Cuk} T_s (D_{Cuk} + D_1)}{2L_{o1}} + i \tag{15}$$

where "I" indicates the current in both the input and output inductors during DCM operation, as seen in Fig. 6. The sum of the inductor currents generated by (14) and (15) yields diode current.

$$\begin{aligned} i_{D_{o1}} &= i_{Li1} + i_{Lo1} = \frac{V_s D_{Cuk} T_s (D_{Cuk} + D_1)}{2} \left(\frac{1}{L_{i1}} + \frac{1}{L_{o1}} \right) \\ &= \frac{V_s D_{Cuk} T_s (D_{Cuk} + D_1)}{2L_{eq}} \end{aligned} \tag{16}$$

where L_{eq} denotes the parallel combination of L_{i1} and L_{o1} .

$$L_{eq} = \left(\frac{L_{i1} L_{o1}}{L_{i1} + L_{o1}} \right) \tag{17}$$

Substituting i_{Lo1} 's value from the power balance equation $V_{spkiLi1} = VC_{ukiLi1}$ as

$$i_{Lo1} = \frac{D_1}{D_{Cuk}} i_{Li1} \tag{18}$$

(16) becomes

$$i_{Li1} = \frac{V_s D_{Cuk}^2 T_s}{2L_{eq}} \tag{19}$$

As a result, the expression for the current via the input inductor is recast as $V_s = V_{spk} \sin \omega t$.

$$i_{Li1} = \frac{V_s D_{Cuk}^2 T_s}{2L_{eq}} \sin \omega t = KV \sin \omega t_{spk} \tag{20}$$

where K is a constant denoted by

$$K = \frac{D_{Cuk}^2 T_s}{2L_{eq}} \tag{21}$$

It is clear from (21) that all of the variables in (20) reflect constant quantities, with the exception of the peak input voltage V_{spk} . It should also be noticed that the input current ($i_{Li1} = i_s$) exactly follows the input voltage envelope of $V_{spk} \sin(\omega t)$, implying that an inherent unity PF operation is validated for the proposed DCM converter. The following is the design procedure for the proposed PQ enhanced EV charger for charging a 48-V/100-Ah battery. The BL-Cuk converter's output voltage is kept constant at 300 V. The voltage gain of the PFC Cuk converter is calculated using the output voltage, V_{Cuk} , and the peak input voltage, V_{spk} .

$$M = \frac{V_{Cuk}}{V_{spk}} = \frac{300}{220\sqrt{2}} = 0.964 \tag{22}$$

The conduction parameter's value is determined by the inductance L_{eq} , switching time T_s , and load resistance R_{Cuk} , which are provided below.

$$K_e = \frac{2L_{eq}}{R_{Cuk} T_s} \tag{23}$$

where the switching frequency of the converter ($1/T_s$) is set to 20 kHz. The dimensionless variable K_e is a measure of a converter's proclivity to operate in DCM. Large values of K_e result in continuous mode operation, whereas lower values result in discontinuous mode operation for some value of the duty cycle. As a result, for the DCM operation,

$$K_e < K_{ecrit} \tag{24}$$

As a result, K_{ecrit} is affected by the type of converter and the duty cycle of D_{cuk} . To determine the boundary between conduction and DCM, the critical conduction parameter K_{ecrit} is calculated as follows:

$$K_{ecrit} = \frac{1}{2(M+n)^2} = \frac{1}{2(0.964+1)^2} = 0.1296. \tag{25}$$

The value of K_e is chosen to be smaller than the calculated value for the DCM operation, i.e., $K_e = 0.08$ is chosen for this application to estimate the various components. The duty cycle of the Cuk converter for the appropriate output voltage is calculated as

$$D_{Cuk} = \sqrt{2M\sqrt{K_e}} = 0.384 \tag{26}$$

The converter's equivalent inductance L_{eq} is calculated using (23) as

$$L_{eq} = 211.76 \mu\text{H} \tag{27}$$

As a result, an equivalent inductance of 200 H is chosen for this application to assure DCM throughout a large voltage range.

To ensure a steady inductor current throughout the switching cycle, the ripple current in the input inductor is set to 40%. As a result, the calculation for the input inductance $L_{i1,2}$ is as follows:

$$L_{i1,2} = \frac{V_s \times D_{Cuk}}{\Delta i_{Li1,2} \times f_s} = \frac{220 \times 0.384}{0.4 \times (850/311) \times 20000} = 3.86 \text{ mH} \tag{28}$$

where the peak current ripple is assumed to be 40% of the input current, i.e., $i_{Li1} = 0.4 I_s$. As a result, the input inductance is set to 4 mH to assure CCM operation. Using (17) and (27) to provide the DCM-based operation, the minimum output inductance $L_{o1,2}$ is calculated as follows:

$$L_{o1,2} \leq \left(\frac{L_{eq} L_{i1,2}}{L_{eq} - L_{i1,2}} \right) = \frac{4 \times 0.2}{4 - 0.2} \text{ mH} = 0.222 \text{ mH} \tag{29}$$

As a result, the value of the output inductance is set to be smaller than the expected amount, i.e., 0.15 mH, to assure the charger's UPF operation throughout a wide input voltage range.

The suggested converter's input current wave-shaping function is directly affected by the energy transfer capacitor, C1. As a result, the design of this capacitor is constrained by the following constraints: The resonant frequencies f_r of $L_{i1,2}$, $L_{o1,2}$, and C1 must be more than the line frequency f during the proposed converter's operation in respective halves and less than the converter switching frequency, f_s , which ensures the CV across one switching cycle, i.e., $f < f_r < f_s$, such that

$$f_r = \frac{1}{2\pi\sqrt{L_{i1,2} + L_{o1,2}}C_{1,2}} \tag{30}$$

The suggested study considers the resonance frequency f_r to be 1.5 kHz. The voltage rating of this energy transfer capacitor is determined by the voltage sum of the charger's peak input voltage and output voltage. To eliminate any resonance between C1,2 and L_{eq} during each half cycle, the energy transfer capacitor, C1,2, is calculated as

$$C_{1,2} = \frac{1}{\omega_r^2(L_{i1,2} + L_{o1,2})}$$

$$= \frac{1}{(2 \times \pi \times 1500)^2(4 + 0.15) \text{ mH}} = 2.71\mu\text{F} \tag{31}$$

where ω_r is set to $2\pi f_r$ and the energy transfer capacitor value is set to $3\mu\text{F}$ to assure CCM operation.

The power drawn from the mains, which includes the double frequency ripple power (2ω), is denoted as

$$P_i = V_{spk}\sin\omega t \times I_{spk}\sin\omega t = V_s I_s (1 - \cos 2\omega t). \tag{32}$$

IV. CONTROL OF THE PROPOSED EV CHARGER

A. Control of the BL PFC Converter

The proposed BL PFC converter is intended to operate in the DCM mode, which employs voltage-follower mode control. The voltage-follower control is implemented using a PI controller, which moulds the mains current to match the input voltage and ensures that the output of the BL converter remains constant despite significant variations in the input voltage. A voltage sensor is used to detect any variation in voltage (VCuk) caused by an abrupt shift in the main voltage. The voltage measured is compared to the appropriate reference voltage (VCukref). The voltage feedback controller receives the error VCuk. The error signal and control signal created during the kth sampling moment are expressed as

$$VCuke(n) = VCukref(n) - VCuk(n)$$

$$CvCuk(n) = CvCuk(n - 1) + KpCuk \{VCuke(n) - VCuke(n - 1)\} + KiCukVCuke(n)$$

where $KpCuk$ and $KiCuk$ are the tuned proportional and integral gain constants for the PI controller, respectively. Following processing by the PI controller, a control signal $CvCuk$ is initiated, which uses a PWM comparator to vary the duty cycle to deliver the desired output voltage. The control signal, $CvCuk$, is compared to a high-frequency wave, Sc , generated internally at the converter switching frequency, f_s , in the PWM comparator. As seen in Figs. 7 and 8, switching occurs during the corresponding halves.

B. Control of the Flyback Converter

To provide CC charging to the battery under all operational conditions, the flyback converter is regulated by a cascaded dual PI controller at the output. The battery voltage, V_{batt} , is measured and compared to a constant reference voltage, V_{batt} , for this purpose. A voltage PI controller provides the voltage error, V_{batte} . The PI controller output is made to saturate at the maximum charging current limit so that the output of the outer PI controller loop establishes the reference I_{batt} for the current in the inner current loop. For the kth sample instance, the relevant equations for error V_{batte} and PI controller output CV_{batt} are provided as

$$V_{batte}(n) = V_{batt} * (n) - V_{batt}(n)$$

$$CV_{batt}(n) = CV_{batt}(n - 1) + KpV_{batt} \{V_{batte}(n) - V_{batte}(n - 1)\} + KiV_{batt}V_{batte}(n)$$

The voltage PI controller parameters are represented here by K_pV_{batt} and K_iV_{batt} . However, the EV battery's sensed charging current, I_{batt} , is compared to this reference value, and the difference is supplied to the inner current PI controller. When the voltage controller's output is saturated at the reference charging current value and the voltage PI controller loop is turned off. The needed pulses are generated by comparing the current PI controller output to a sawtooth wave to charge the battery in the CC mode using the PWM generating block.

V. RESULTS

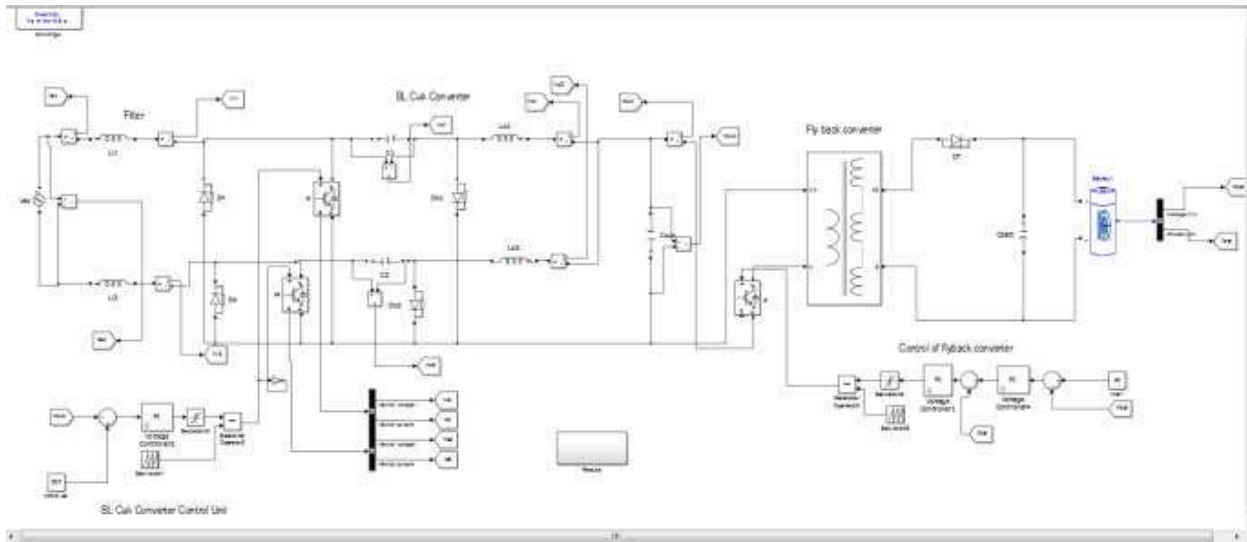


Fig. Simulation circuit.

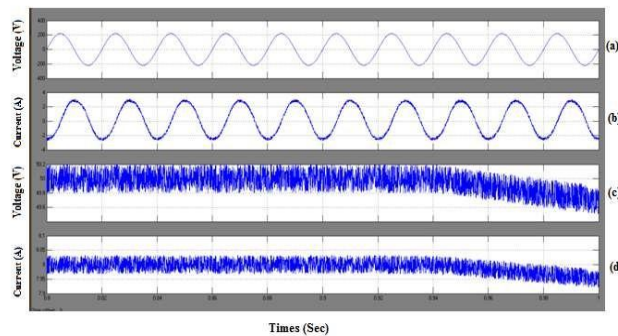


Fig. a. Source and Battery side quantities.

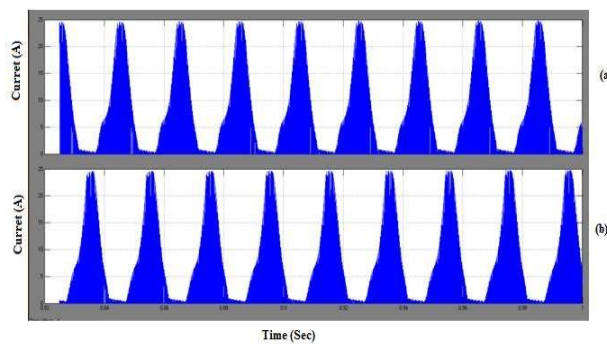


Fig. b. Output inductor current (a) $i_{lo1}=28A$ (b) $i_{lo1}=28A$.

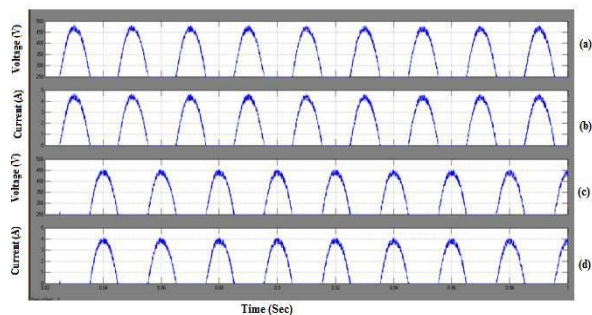


Fig. c. charger Capacitor voltages in CCM
(No return current through Li1 and Li2 in -ve and +ve half respectively).

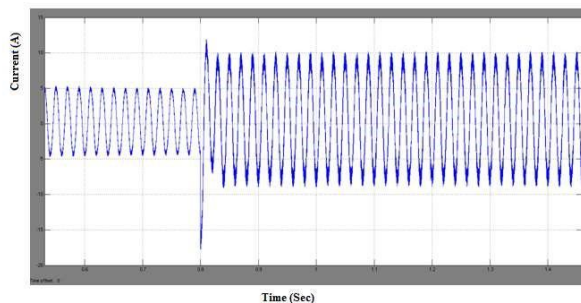


Fig. d. Mains current increased AC mains current (10A).

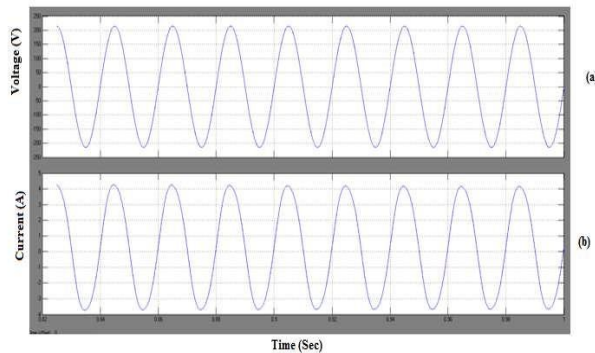


Fig. e. Main voltage and currents.

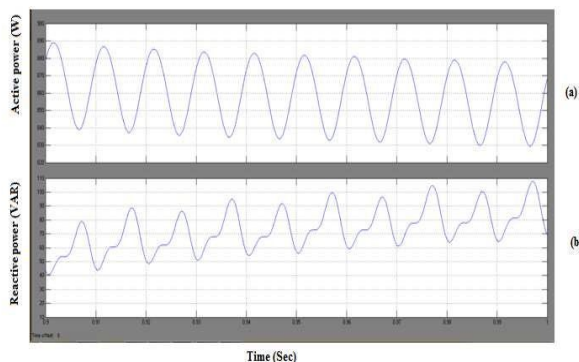


Fig. f. (a)Active power (b)Reactive power

Similarly, there is no return current visible through Li1 during the -ve half cycle, as seen in Fig. 3.6 for the prior BL Cuk converter topology-3 with conventional regulation. It is worth noting that a small number of current flows via Li2 during the +ve half-line of a BL Cuk converter with conventional control, which is acquired due to the path given by the body diode of the inactive switch S2 during the positive half. Similarly, Li1 shows a small amount of current flowing through it during the negative half line because the body diode of the inactive switch S1 is conducting at this time. As a result of the losses experienced by the body diode of the inactive switch, the converter efficiency is seen to be low in Figs. e and f.

VI. CONCLUSION

A better PQ-based EV charger is proposed, featuring a BL Cuk converter that uses fewer conducting components in a single switching cycle. Using a single-voltage feedback control, the proposed PFC Cuk converter provides outstanding PFC characteristics in the DCM mode. As a result, the charger's size is lowered. The suggested topology also eliminates the undesired capacitive coupling loop, as well as the unwanted conduction through the body diode of the inactive switch in the previously developed BL Cuk converter. This enhances the charger's efficiency greatly. The proposed charger demonstrated good charging behaviour at the steady state and during a 50% change in grid voltage. However, the proposed charger's PQ assessment is accomplished using the IEC 61000-3-2 guidelines over a large input voltage range. As a result, the suggested charger provides a viable EV charging alternative for increased PQ and efficiency.

REFERENCES

- [1] C. Chan and K. Chau, "Power electronics challenges in electric vehicles," in Proc. 19th Annu. Conf. IEEE Ind. Electron., 1993, pp. 701–706.
- [2] B. Tar and A. Fayed, "An overview of the fundamentals of battery chargers," in Proc. IEEE 59th Int. Midwest Symp. Circuits Syst., 2016, pp. 1–4.
- [3] M. Yilmaz and P. T. Krein, "Review of battery charger topologies, charging power levels, and infrastructure for plug-in electric and hybrid vehicles," IEEE Trans. Power Electron., vol. 28, no. 5, pp. 2151–2169, May 2013.
- [4] S. S. Williamson, A. K. Rathore, and F. Musavi, "Industrial electronics for electric transportation: Current state-of-the-art and future challenges," IEEE Trans. Ind. Electron., vol. 62, no. 5, pp. 3021–3032, May 2015.
- [5] Limits for Harmonics Current Emissions (Equipment current ≤ 16 A per Phase), International standards IEC 61000-3-2, 2000.
- [6] F. Musavi, M. Edington, W. Eberle, and W. G. Dunford, "Evaluation and efficiency comparison of front-end AC-DC plug-in hybrid charger topologies," IEEE Trans. Smart Grid, vol. 3, no. 1, pp. 413–421, Mar. 2012.
- [7] H. Choi, "Interleaved boundary conduction mode (BCM) buck power factor correction (PFC) converter," IEEE Trans. Power Electron., vol. 28, no. 6, pp. 2629–2634, Jun. 2013.
- [8] Y. Hsieh, T. Hsueh, and H. Yen, "An interleaved boost converter with zero-voltage transition," IEEE Trans. Power Electron., vol. 24, no. 4, pp. 973–978, Apr. 2009.
- [9] C. Li and D. Xu, "Family of enhanced ZCS single-stage single-phase isolated AC-DC converter for high-power high-voltage DC supply," IEEE Trans. Ind. Electron., vol. 64, no. 5, pp. 3629–3639, May 2017.
- [10] S. Chen, Z. R. Li, and C. Chen, "Analysis and design of single-stage AC/DC LLC resonant converter," IEEE Trans. Ind. Electron., vol. 59, no. 3, pp. 1538–1544, Mar. 2012.
- [11] S. Lee, W. Cha, and B. Kwon, "High-efficiency soft-switching AC-DC converter with single-power-conversion method," IEEE Trans. Ind. Electron., vol. 64, no. 6, pp. 4483–4490, Jun. 2017.
- [12] D. H. Kim, M. J. Kim, and B. K. Lee, "An integrated battery charger with high power density and efficiency for electric vehicles," IEEE Trans. Power Electron., vol. 32, no. 6, pp. 4553–4565, Jun. 2017.
- [13] C. Shi, Y. Tang, and A. Khaligh, "A single-phase integrated on-board battery charge using propulsion system for plug-in electric vehicles," IEEE Trans. Veh. Technol., vol. 66, no. 12, pp. 10899–10910, Dec. 2017.
- [14] M. M. Jovanovic and Y. Jang, "State-of-the-art, single-phase, active power-factor-correction techniques for high-power applications— An overview," IEEE Trans. Ind. Electron., vol. 52, no. 3, pp. 701–708, Jun. 2005.
- [15] L. Petersen and M. Andersen, "Two-stage power factor corrected power supplies: The low component-stress approach," in Proc. IEEE Appl. Power Electron. Conf., 2002, vol. 2, pp. 1195–1201.
- [16] B. Singh, B. N. Singh, A. Chandra, K. Al-Haddad, A. Pandey, and D. P. Kothari, "A review of single-phase improved power quality ACDC converters," IEEE Trans. Ind. Electron., vol. 50, no. 5, pp. 962–981, Jul. 2003.
- [17] B. Zhao, A. Abramovitz, and K. Smedley, "Family of bridgeless buck boost PFC rectifiers," IEEE Trans. Power Electron., vol. 30, no. 12, pp. 6524–6527, Dec. 2015.
- [18] R. Kushwaha and B. Singh, "An improved battery charger for electric vehicle with high power factor," in Proc. IEEE Ind. Appl. Soc. Annu. Meet., 2018, pp. 1–8.
- [19] D. S. L. Simonetti, J. Sebastian, F. S. dos Reis, and J. Uceda, "Design criteria for SEPIC and Cuk converters as power factor pre-regulators in discontinuous conduction mode," in Proc. Int. Conf. Ind. Electron., Control, Instron., Autom., 1992, vol. 1, pp. 283–288.
- [20] A. A. Fardoun, E. H. Ismail, A. J. Sabzali, and M. A. Al-Saffar, "New efficient bridgeless Cuk rectifiers for PFC applications," IEEE Trans. Power Electron., vol. 27, no. 7, pp. 3292–3301, Jul. 2012.
- [21] M. R. Sahid, A. H. M. Yatim, and N. D. Muhammad, "A bridgeless Cuk PFC converter," in Proc. IEEE Appl. Power Electron. Colloq., 2011, pp. 81–85.
- [22] A. J. Sabzali, E. H. Ismail, M. A. Al-Saffar, and A. A. Fardoun, "New bridgeless DCM sepic and Cuk PFC rectifiers with low conduction and switching losses," IEEE Trans. Ind. Appl., vol. 47, no. 2, pp. 873–881, Mar./Apr. 2011.
- [23] M. Mahdavi and H. Farzaneh-Fard, "Bridgeless CUK power factor correction rectifier with reduced conduction losses," IET Power Electron., vol. 5, no. 9, pp. 1733–1740, Nov. 2012.
- [24] R. Kushwaha and B. Singh, "A power quality improved EV Charger with bridgeless Cuk converter," in Proc. IEEE Power Electron., Drives Energy Syst., 2018, pp. 1–6.
- [25] A. Jha and B. Singh, "Bridgeless zeta PFC converter for low voltage high current LED driver," in Proc. IEEE CERA, 2017, pp. 539–544.
- [26] SAE Electric Vehicle and Plug-in Hybrid Electric Vehicle Conductive Charge Coupler, SAE Standard J1772, 2010.
- [27] C. Zhao, J. Zhang, and X. Wu, "An improved variable on-time control strategy for a CRM flyback PFC converter," IEEE Trans. Power Electron., vol. 32, no. 2, pp. 915–919, Feb. 2017.



- [28] K. Yao, X. Ruan, X. Mao, and Z. Ye, "Variable-duty-cycle control to achieve high input power factor for DCM boost PFC converter," *IEEE Trans. Ind. Electron.*, vol. 58, no. 5, pp. 1856–1865, May 2011.
- [29] T. J. Liang, K. H. Chen, and J. F. Chen, "Primary side control for flyback converter operating in DCM and CCM," *IEEE Trans. Power Electron.*, vol. 33, no. 4, pp. 3604–3612, Apr. 2018.
- [30] S.F.Lim and A.M. Khambadkone, "A simple digital DCM control scheme for Boost PFC Operating in both CCM and DCM," *IEEE Trans. Ind. Appl.*, vol. 47, no. 4, pp. 1802–1812, Jul./Aug. 2011.
- [31] B. Abdi, A. H. Ranjbar, J. Milimonfared, and G. B. Gharehpetian, "Reliability comparison of boost PFC converter in DCM and CCM operating modes," in *Proc. IEEE Int. Symp. Power Electron., Elect. Drives, Autom. Motion*, 2008, pp. 939–943.
- [32] L. Wang, Q.H. Wu, W.H. Tang, Z.Y. Yu, and W. Ma, "CCM-DCM average current control for both continuous and discontinuous conduction modes boost PFC converters," in *Proc. IEEE Elect. Power Energy Conf.*, 2017, pp. 1–6.



10.22214/IJRASET



45.98



IMPACT FACTOR:
7.129



IMPACT FACTOR:
7.429



INTERNATIONAL JOURNAL FOR RESEARCH

IN APPLIED SCIENCE & ENGINEERING TECHNOLOGY

Call : 08813907089  (24*7 Support on Whatsapp)